Desalination and Water Treatment
www.deswater.com
doi: 10.1080/19443994.2015.1072739

57 (2016) 15265–15275
July

Taylor & Francis
Taylor & Francis Group

Integration of CFD and RTD analysis in flow pattern and mixing behavior of rotary pressure exchanger with extended angle

Zheng Cao, Jianqiang Deng*, Wenjun Yuan, Zhihua Chen

School of Chemical Engineering and Technology, Xi'an Jiaotong University, Xi'an, Shaanxi 710049, China, email: czczkok@stu.xjtu.edu.cn (Z. Cao), Tel./Fax: +86 29 82663413; emails: dengjq@mail.xjtu.edu.cn (J. Deng), yuanwenjun.347@stu.xjtu.edu.cn (W. Yuan), czh1991.0913@stu.xjtu.edu.cn (Z. Chen)

Received 1 October 2014; Accepted 4 July 2015

ABSTRACT

In this study, the computational fluid dynamics (CFD) approach combined with the residence time distribution (RTD) analysis was implemented to examine the mixing performance and flow pattern of rotary pressure exchanger (RPE). Based on oscillatory Reynolds number, a flow regime classification was established for RPE. A concept of extended angle of RPE was proposed, and then, its effects on mixing behavior were evaluated by CFD simulation in laminar model. Meanwhile, flow pattern in RPE was quantified by RTD study, and was well captured in the flow field analysis. In addition, the effects of operating conditions on the mixing and flow pattern were discussed. According to the results, it was shown that the extended angle of RPE is beneficial for mixing control, and a minimum volumetric mixing rate was achieved when the extended angle is ±30° compared with other configurations. In different operating conditions, the mixing rate was minimized at an oscillatory Reynolds number of about 178. Moreover, the smaller RTD variance, the closer was the flow pattern to an ideal plug flow, leading to a lower volumetric mixing rate of RPE. This study indicates that the RTD and CFD simulation are capable for mixing study and flow analysis in RPE device, and they are complementary and verifiable with each other.

Keywords: Rotary pressure exchanger; SWRO system; Numerical simulation; Flow pattern; Mixing

1. Introduction

The demand of water resources is still increasing with the development of human society, and the global population living in water-stressed regions is estimated to reach 3.5 billion by 2025 [1,2]. Seawater reverse osmosis (SWRO), as the most efficient technology in seawater desalination [3], has shifted people's attention from overexploited groundwater to abundant seawater resources. In this technology, the application of isobaric energy recovery devices (ERDs) decreases the energy consumption by up to 60%, making the production of freshwater economical with low carbon emission [4]. By far, more than 80% of newly built SWRO plants are utilizing Isobaric ERDs [5].

Rotary pressure exchanger (RPE), as one kind of isobaric ERDs, has attracted increasing interest for its unique advantages including maintenance-free operation, flexible capacity, ease of control, and high energy recovery efficiency (up to 98%). Due to these remarkable features, RPE has been applied in worldwide

*Corresponding author.

desalination plants such as Hadera plant, which is one of the largest SWRO plants with an expanded production capacity of 150 million cubic meters annually [6]. Moreover, the promising application of RPE can also be extended to other membrane processes where the pressure of concentrate stream needs to be recovered. Interestingly, it has been already employed in a conceptual process design for juice concentrate production, in order to reduce the power consumption of the flow system [7].

The working principle of RPE is simple: pressure energy is transferred between two liquids by following Pascal's law which states that the applied pressure on a confined liquid is to transmit uniformly in all directions. As shown in Fig. 1, high pressure brine flows into a rotor with a plurality of open-ended ducts. Meanwhile, seawater in the duct has been instantaneously pressurized and pushed out. When the duct rotates to low pressure side, fresh seawater fills in the duct and displaces the depressurized brine reversely. A continuous pressure exchange is accomplished with this periodic process. However, during the pressure transfer process, mixing of brine and seawater occurs inevitably due to the direct contact between the two fluids. In SWRO system, a 2.5% increase in salinity at the membrane will lead to an increase of operating pressure by 0.13 MPa [8]. As a result, the energy consumption will rise. For the potential application in any other process industries, the purity of pressurized fluid in RPE also needs to be guaranteed. Therefore, the mixing control is a key issue to improve the RPE performance.

Several researchers have studied the mixing behavior of RPE. Zhou et al. [9,10] simulated the concentration distribution in RPE using k–ε model, and obtained the effects of rotor parameters and operating conditions on the mixing performance. It was found that the length of mixing zone had a maximum value at optimization of the duct quantity and length. Also, the mixing intensified with an increase in flow rate and a decrease in rotation speed. Xu et al. [11] also carried out a simulation of mixing in RPE with the turbulence model. A second-order polynomial relationship between the mixing rate and the dimensionless inflow length was obtained, and was validated by an experiment. Considering the duct flow as laminar, Mei et al. [12] performed a theoretical calculation to predict the longitudinal dispersion of salt along each duct of RPE. Assumed that the flow velocity was inputted as series of rounded rectangles, the spreading time and the amount of salt that transferred inside the duct was estimated. To prevent the mixing, Al-Hawaj [13] presented an RPE structure which contains a sliding ball piston as the physical barrier in each duct. However, this design is difficult to realize practically because ducts and pistons are prone to wear during the continuous friction process.

Although some work has been done on mixing evaluation of RPE by numerical method and theoretical approximation, the specific assessment of flow characters and its inherent relationship with mixing performance have not yet been performed, and an accurate simulation with appropriate model is still necessary to provide detailed flow information in RPE. Hence, in this work, the flow pattern and mixing behavior of RPE were investigated. A flow regime classification was developed before numerical study. On this basis, the laminar model was implemented in a three-dimensional CFD simulation. Mixing performance of RPE with different extended angles has been evaluated. Besides, flow pattern of RPE was quantified through residence time distribution (RTD) analysis, and was well captured in the flow field analysis. In addition, the effects of operating conditions on the mixing and flow pattern of RPE were also discussed. The aim of this work is to study the effects of flow pattern on RPE mixing performance, and to propose an optimal method for mixing control from a new perspective.

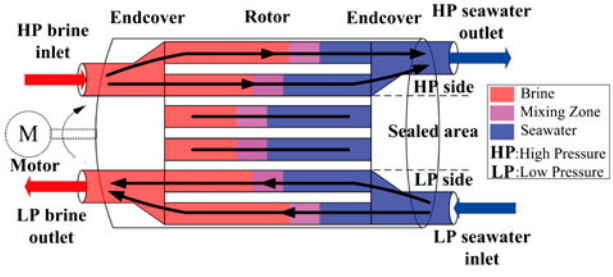

Fig. 1. Working schematic diagram of RPE.

2. Flow regime

For most pipe flow, the transition from laminar flow to turbulence occurs at a Reynolds number of 2,300. However, many researchers found that this kind of unidirectional steady flow is less stable compared with purely oscillatory pipe flow [14]. Due to the special flow features of RPE device, the continuous outlet streams are composed of series of reciprocating oscillatory flows in each duct. The criterion for transition in RPE device needs to be reconsidered.

The Reynolds number for oscillatory pipe flow can be written as:

$$Re_\delta = \frac{(u \cdot \delta_{st})}{\upsilon} \quad (1)$$

where u is the mean velocity, and υ is the kinematic viscosity. The stokes' layer thickness is:

$$\delta_{st} = \sqrt{\frac{2\upsilon}{\varpi}} \quad (2)$$

where ϖ is the oscillation frequency.

Since the flow is injected into each duct periodically with rotation, the frequency of oscillating motion can be related to rotation period. Experiments on transitional flow structure of oscillatory pipe flow were carried out and the critical Reynolds numbers Re_c were investigated by several researchers [14–17]. As shown in Fig. 2, four curves represent transition lines based on experimental critical Reynolds numbers. Flow structure in a regime below the line is more close to laminar flow, while it becomes turbulent above the line at a high velocity or low rotation speed. Although the values of critical Reynolds numbers are slightly different, they are of same magnitude in observation. In common operating conditions of RPE, the rotary speed ranges from 500 to 2,000 r/min [8], and the inflow velocity is mostly below 4 m/s with a flow rate between 4.5 and 60 m^3/h [18,19]. Based on the transition criterion of oscillatory flow, the duct flow is more close to a laminar flow, this is in agreement with the literature [12]. In the present study, the maximum rotary speed is set to 1,200 rpm and the inflow velocity is no larger than 2.5 m/s. Therefore, flow regime under this operating condition is laminar flow according to the critical Reynolds number.

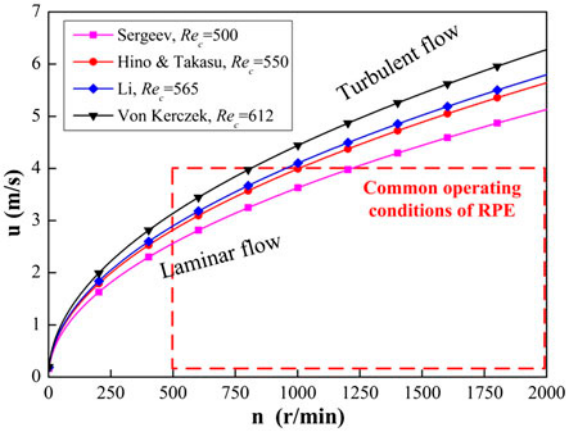

Fig. 2. Flow regime transition lines in RPE.

3. Numerical study

3.1. CFD model

In accordance with the flow regime for the given working conditions, laminar model has been chosen to close the governing equations:

Mass conservation:

$$\frac{\partial \rho}{\partial t} + \nabla \cdot (\rho \vec{v}) = 0 \quad (3)$$

Momentum equation:

$$\frac{\partial}{\partial t}(\rho \vec{v}) + \nabla \cdot (\rho \vec{v}\vec{v}) = -\nabla p + \nabla \cdot \tau + (\rho \vec{g} + \vec{F}) \quad (4)$$

Species transport equation:

$$\frac{\partial}{\partial t}(\rho Y_i) + \nabla \cdot (\rho \vec{v} Y_i) = -\nabla \vec{J}_i \quad (5)$$

where J_i is the mass diffusion flux of species i, which is determined by Fick's law for laminar flows:

$$J_i = -\rho D_{i,m} \nabla Y_i \quad (6)$$

In equations above, ρ is the density, $\vec{v}$ is the velocity vector, p is the static pressure, τ is the tension tensor, $\vec{g}$ is the gravity constant, $\vec{F}$ is the external volume force, and Y_i is the mass fraction for species i.

As effective diffusion coefficient consists of molecular diffusion coefficient and convective diffusion coefficient, it is worthwhile mentioning that the diffusion of NaCl in aqueous solution begins with salt dissociation. However, the interionic attraction between sodium ion and chloride ion makes the independent diffusion of each ion equivalent to the diffusion of the ion pair. For this reason, the mass diffusivity of species NaCl is set to a constant value of 1.5e−9 m^2/s [20]. This diffusion effect should not be neglected for most laminar flow at low Reynolds number.

The simplified geometric model is shown in Fig. 3. Main geometrical parameters include duct length l = 150 mm, end cover height H = 10 mm, duct diameter d = 15 mm, and rotor radius R = 40 mm. In Fig. 3, the inlet in endcover is extended by an angle compared with outlet. The angles α and β are defined as extended angles. For convenience to identify, α is given to a positive value which implies the duct contacts with the extended inlet before connecting to the outlet, whereas β is given to a negative value which

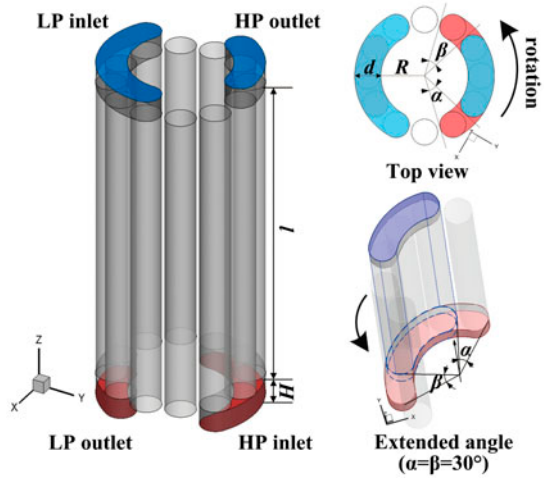

Fig. 3. Simulated domain of RPE.

means that the duct rotates out of the outlet while still exposing to the inlet. In this figure, the extended angle is written as ±30˚, suggesting the inlet has just covered one more duct in both sides. In order to make a comparison for the mixing performance of RPE, different configurations are built with an extended angle of 0˚, 7.5˚, 15˚, 22.5˚, 30˚, and ±30˚ respectively.

In Fig. 4, the unstructured grid is used to discretize the computational domain, as shown in Fig. 4. The RPE model consists of 1,208,717 nodes and 1,154,100 cells with a finely meshed grid by Gambit tool. All ducts in rotor are connected with endcovers through interface on the assumption that no gap exists and therefore no leakage happens between each duct. The moving mesh method is selected for ducts to achieve the stable rotation provided by external driving force.

The differential equations are solved by commercial CFD software Fluent 6.3a, which is a widely used solver depending on the finite volume method. An unsteady, incompressible flow is considered in the numerical analysis. The inlet velocity is specified for both HP saline water and LP seawater inflow with a flow rate of 5.0 m^3/h, and pressure boundary conditions of 6.0 and 0.2 MPa are used at HP outlet and LP outlet, respectively. In addition, the NaCl concentration of brine is set to 6.5%, and the concentration of fresh seawater is set to 3.5%. To achieve a stable rotation of RPE, the rotor speed is assigned as 1,000 rpm.

The preliminary settings of geometric parameters and operating parameters satisfy the following criterion:

$$L_m < l \tag{7}$$

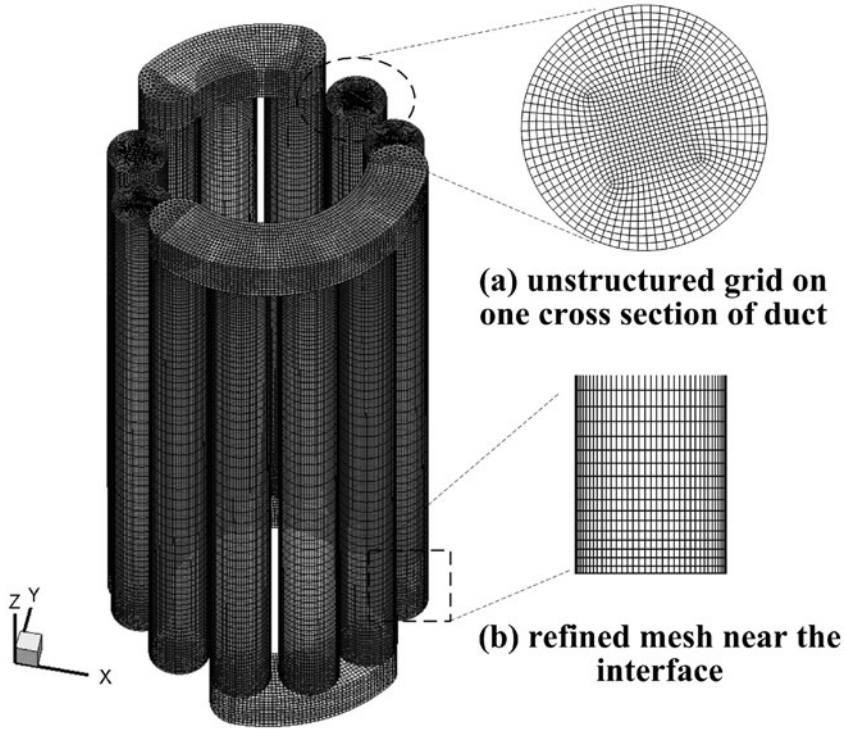

Fig. 4. Meshed grid system of computational flow domain.

where L_m is the inflow length of high concentrate flow, which can be calculated based on the mass balance in a steady-state flow condition, as shown below:

$$L_m = \frac{Q}{A_1} = \frac{v \cdot A_1 \cdot (\varphi_1/\varpi) + 2v \cdot A_2 \cdot (\varphi_2/\varpi)}{A_1} \tag{8}$$

where Q, v, and ω are the flow rate entering the duct, the inflow velocity, and the rotating speed, respectively. During the duct rotation, φ_1 represent the rotation angle when duct is fully connected to the endcover, and φ_2 represent the central angle of a single duct. A_1 and A_2, respectively, represent the cross area of each duct and the effective flow area during duct switching in process. Under the given operating condition, the theoretical L_m is estimated to be 0.02 m, which is much smaller than the duct length.

3.2. Flow pattern characterization

The flow pattern of fluids in chemical process has a significant effect on mass transfer performance. Considering the unsteady characters and the non-uniform velocity distribution in most flowing systems, fluid elements spend different time in flowing through the system. By monitoring the amount of fluid elements at the outlet vs. time, the RTD can be obtained. In the analysis of numerical characteristics of RTD, it is helpful to reveal flow characters and mixing performance of the process. The technology of RTD analysis was first introduced by Danckwerts to study the non-ideal flow behaviors of chemical reactors [21], and now it has been widely applied in continuous flow systems such as chemical and petrochemical process, food processing system, environmental monitoring, and metallurgy industry. The general applicability and quantitative feature make it an efficient method to evaluate flow characters for unsteady and complicated flow.

The RTD data are acquired by measuring tracer concentration at the outlet of a flow system. The most common tracer injection methods include pulse, step, and periodic input. For RPE device, brine stream flows into HP inlet at a constant rate. Therefore, in this study, the 6.5% NaCl is adopted as numerical tracer by a step input method. The accumulative RTD function $F(t)$ represents the fraction of outflowing tracers, and it is given by the following equation:

$$F(t) = \frac{c(t_i)}{c_0} \tag{9}$$

where $c(t_i)$ is the concentration of tracer in the outlet stream, and c_0 is the constant concentration of the injected stream.

The RTD density function $E(t)$ is the distribution of times of the tracers leaving the system for the length of time between t and $t + dt$, which can be calculated as follows:

$$E(t) = \frac{\mathrm{d}F(t)}{\mathrm{d}t} \tag{10}$$

Once the RTD function is obtained, some important digital features can be calculated for the quantitative description on the flow pattern.

The mean residence time τ represents the average time the outflowing tracers spend in the flow system. It is the first moment of the RTD which can be determined by the following equation:

$$\tau = \int_0^\infty tE(t)\,dt \approx \sum_{i=0}^{\infty} t_i E(t_i)\Delta t_i \tag{11}$$

The variance σ_t^2 measures the extent of the spread of the distribution, which is an important index to evaluate the flow pattern. It is the second moment of the RTD, as shown below:

$$\sigma_t^2 = \int_0^\infty (t-\tau)^2 E(t)\,dt \approx \sum_{i=0}^{\infty} (t_i-\tau)^2 E(t_i)\Delta t_i \tag{12}$$

In order to make a parametric RTD analysis in different flow configurations and operating conditions, the dimensionless time θ is introduced:

$$\theta = \frac{t}{\tau} \tag{13}$$

A normalized RTD function is then given by:

$$E(\theta) = \tau E(t) \tag{14}$$

And the normalized variance of RTD is:

$$\sigma_\theta^2 = \frac{\sigma_t^2}{\tau^2} \tag{15}$$

A normalized variance approaching to zero suggests that an almost ideal plug flow is achieved. While a normalized variance close to one indicates that there is a severe longitudinal mixing caused by non-uniform

velocity distribution and diffusion, and the flow pattern is close to a perfectly mixed flow.

3.3. Mixing performance characterization

In isobaric RPE device, axial mixing of brine stream and seawater stream is inevitable due to the continuous contact of two fluids. The degree of mixing in RPE device is reflected by volumetric mixing rate V_m, which is defined as:

$$V_m = \frac{S_{HO} - S_{LI}}{S_{HI} - S_{LI}} \tag{16}$$

where S_{HO} is the salinity of the pressurized seawater at high pressure outlet, S_{LI} is the salinity of fresh seawater at low pressure inlet, and S_{HI} represents the salinity of incoming brine at high pressure inlet. In this equation, the mixing behavior at low pressure outlet is less concerned. This is because the pressurized seawater will be circulated in the membrane process, and will influence the membrane performance in SWRO system. Meanwhile, waste brine is discharged after the pressure recovery process is finished, and it will not enter the membrane system again.

4. Model validation

A numerical validation has been made using a 4-port RPE with 0 extended angles presented in the literature [11]. As the parameters are not all provided, the model parameter settings follow approximately the experimental conditions. As the rotor size, duct size, mass fraction of NaCl, flow rate, and rotary speed are known, we assume that the high pressure outlet is 6.0, and 0.1 MPa. It is mentioned that although the validation model and RPE models in our work are of different sizes, the working principle and pressure exchange process are identical. Therefore, the validation results can be used to confirm the accuracy of the numerical model used in our simulation.

In Fig. 5, the calculated volumetric mixing rates have been compared with the corresponding experimental data in different operating conditions. The ratio of inflow length and duct length is defined as the dimensionless inflow length, and it is slightly smaller in simulation results than that in experimental data. Besides, the curves of numerical result and experimental data follow a similar trend, and the values of mixing rate are in a good agreement with a ±10% range of the percentage relative error. This outcome therefore makes an acceptable quantitative validation of the numerical model used in this work.

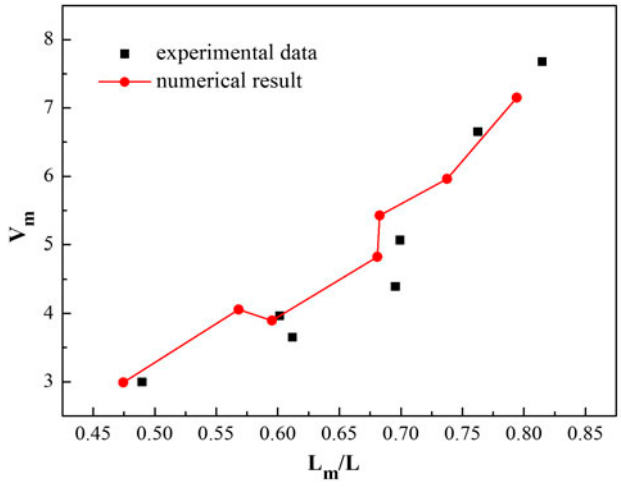

Fig. 5. Comparison between the numerical results and experimental data in Ref. [11].

5. Results and discussion

5.1. Mixing formation

Fig. 6 shows the mixing formation process of RPE with different extended angles. Since the RTD functions are obtained based on the tracer concentration vs. time data, a liner relationship is observed between the volumetric mixing rate V_m and the accumulative RTD function $F(t)$. All curves exhibit a similar trend, which is expected to characterize the mixing formation process. As the high concentration of NaCl is injected into the HP inlet and RPE starts to rotate, the mixing process increases rapidly after a small delay, and then slows down until a relevant steady mixing is formed at about 2.0 s. It is found that the effects of various extended angles on mixing performance become

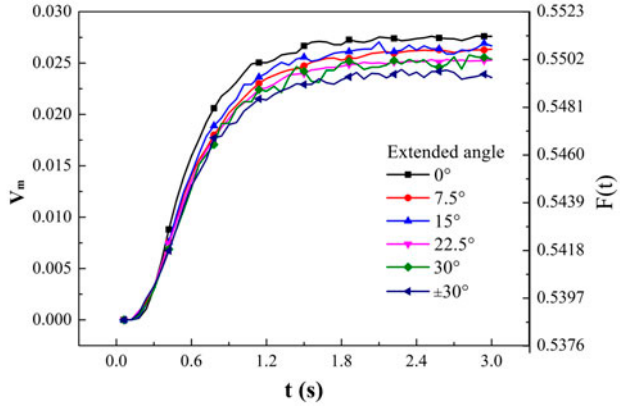

Fig. 6. Mixing formation process of RPE with different extended angles.

obvious at about 0.6 s. Thereafter, the overall V_m of ±30° case appears to remain at the lowest level, whereas the 0° case seems to keep a highest V_m.

5.2. Flow pattern

For various RPE configurations with different extended angles, the average V_m and the normalized variance of RTD are presented in Fig. 7. These two parameters, indicating mixing performance and flow pattern, respectively, show a good accordance with each other. This implies that in RPE, the smaller the normalized variance, that is, the closer the flow pattern adjusts to plug flow, and the smaller the volumetric mixing effect will be. It can be well explained that mixing occurs in ducts of RPE when the brine and seawater make a contact and axial dispersion is enhanced due to non-uniform velocity profile and molecular diffusion; however, the plug flow pattern has a relative plane velocity distribution which will keep concentration of two streams separated only if the piston-shaped interface is disordered or expelled from of HP outlet. Besides, Fig. 7 also confirms that the ±30° case has the lowest V_m and smallest variance in all configurations, and the variance may be regarded as an indicator of the extent of mixing in RPE as well as volumetric mixing rate. Therefore, optimizing flow pattern to a plug flow is effective for mixing control.

As contained much flow information over time, Fig. 8 gives the distributions of the normalized RTD function for the two extreme cases at a maximum V_m and a minimum V_m. In this figure, it is found that the overall E curve of ±30° case is narrower than that of the 0° case, and a lower peak point suffers a displacement to the right and deviates less from the mean residence time. These are implying that ±30° case

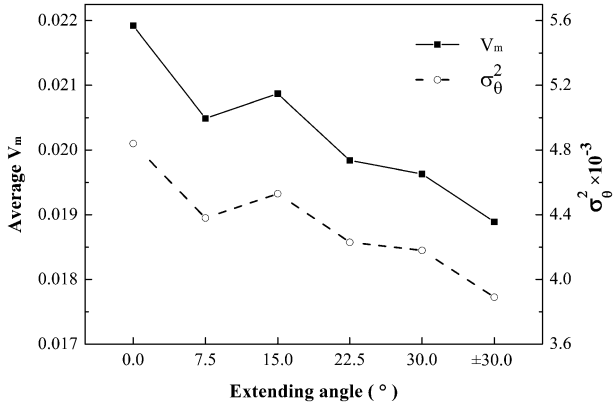

Fig. 7. Comparison of mixing performance and flow pattern between various extended angles.

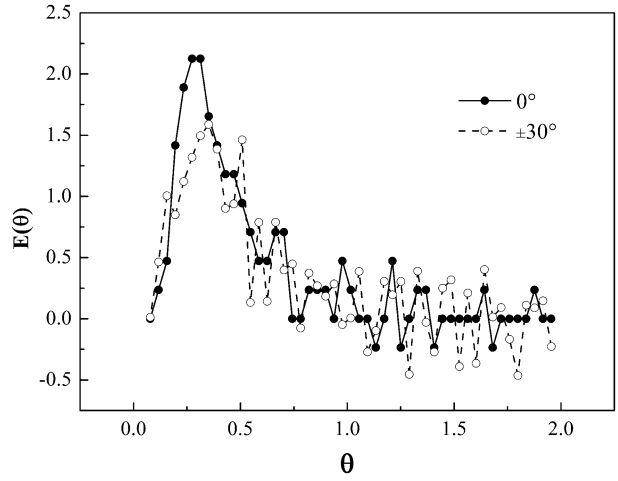

Fig. 8. Normalized RTD function various with dimensionless time in 0° and ±30° cases.

approaches the plug flow behavior and 0° case tends to have a stronger mixing. In a flow system, a dead volume refers to a slow moving or completely stagnant region, while a backflow zone is a region where the velocity direction of fluid is opposite to its inflow direction. As is shown in Fig. 8, both RTD curves fluctuate around zero with a long tail after the mean residence time, indicating that there might be a dead volume and backflow in RPE device. This oscillating tailing phenomenon can be easily understood if considering the working process of RPE. After the steady mixing state achieved, the concentration of brine inflow and seawater inflow reaches a balance. The numerical tracer is entrained by the HP inlet flow, however, a large part of it is trapped in the sealed area with the rotor rotation, and some of it is then rejected by the inverse LP inflow, the numerical tracer in the mixing zone reciprocates in each cycle, therefore the E curve shows up-and-down fluctuations.

5.3. Flow field in RPE

Fig. 9 shows the streamlines colored by velocity on HP side at a time of 2.403 s. As shown in Fig. 9(a), the duct just entering the HP side (first from left) has a strong rotating flow caused by duct rotation and periodic rotor–stator interaction, the streamlines are more disordered compared with Fig. 9(b). Another conspicuous difference lies in the duct just leaving the HP side (first from right), an intense laminar jet flow is formed in duct inlet due to the sudden closure of HP inlet with a zero extended angle. This figure illustrates that the non-ideal flow structures could be eliminated by extending inlet in both directions.

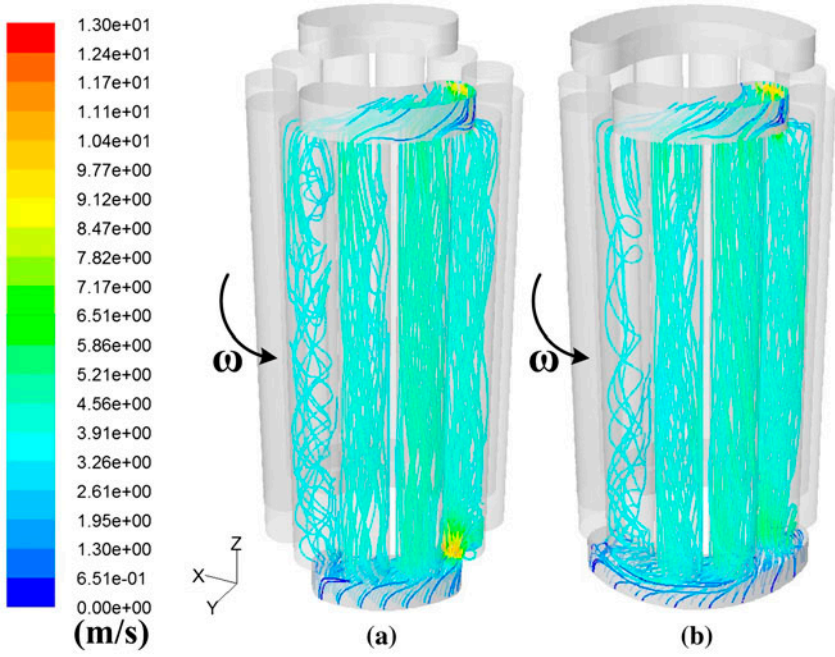

Fig. 9. Streamline of RPE device with an extended angle of 0° (a) and ±30° (b).

In order to observe flow pattern and mixing inside RPE, the axial velocity vectors and concentration fields on internal cylinders at a time of 3 s are illustrated in Fig. 10. The cylinders pass through all duct axes, and are extended along I–I and II–II directions, respectively. The rotation around axis z has therefore been transformed into a two-dimensional motion from left to right. Considering the symmetry of the model structure and reverse inflow of RPE, axial velocity vectors of high pressure side and concentration distribution of low pressure side are shown together in one picture.

In Fig. 10, it is seen that the velocity distribution is relatively uniform in connected area. During the duct rotation from connected area to sealed area, a laminar jet flow is formed. Meanwhile, the fluid close to sealed area becomes almost static, and its velocity is inclined to reverse when subjects to a shear force, this results in a recirculation. In sealed area, fluids are in a stationary state in the dead volume (marked as D) except for the recirculation region (marked as R). In addition, the concentration field can be divided into three regions: brine of high NaCl concentration, mixing zone, and seawater of low NaCl concentration. They are in a relatively fixed position in sealed area, and are propelled forward in flow direction in connected area. Through comparison, the velocity profile in Fig. 10(a) is more uneven in connected area than that in Fig. 10(b), and a more distinct and longer recirculation region is observed when the duct is entering the sealed area. This phenomenon might be caused by the sudden connection of duct ends to endcover inlet and outlet, initiating a velocity disturbance or swirling motion under a big pressure gradient. In the configuration with an extended angle of ±30°, the endcover inlet is connected to the duct ahead of the endcover outlet, and begins to separate until the duct is fully sealed. Therefore, the dramatic change in pressure and flow velocity will not happen simultaneously, and the duct flow is more close to a plug flow in this case. As the concentration distribution is affected by velocity field, a smoother and shorter mixing zone is observed in Fig. 10(b), which makes contribution to a lower mixing rate in RPE device.

5.4. Effects of operating conditions

The operating parameters such as rotary speed and inflow velocity have a great effect on the mixing rate of RPE. In the 1D simplified analysis for inflow length of RPE, it is implied that the mixing rate could be decreased by increasing rotary speed or by decreasing inflow velocity. However, the flow field in RPE is extremely complex, and the concentrate can be affected by many unsteady flow structures such as laminar jet, swirl flow or recirculation flow. In some operating conditions, the effects of rotary speed and inflow velocity on mixing rate may be different.

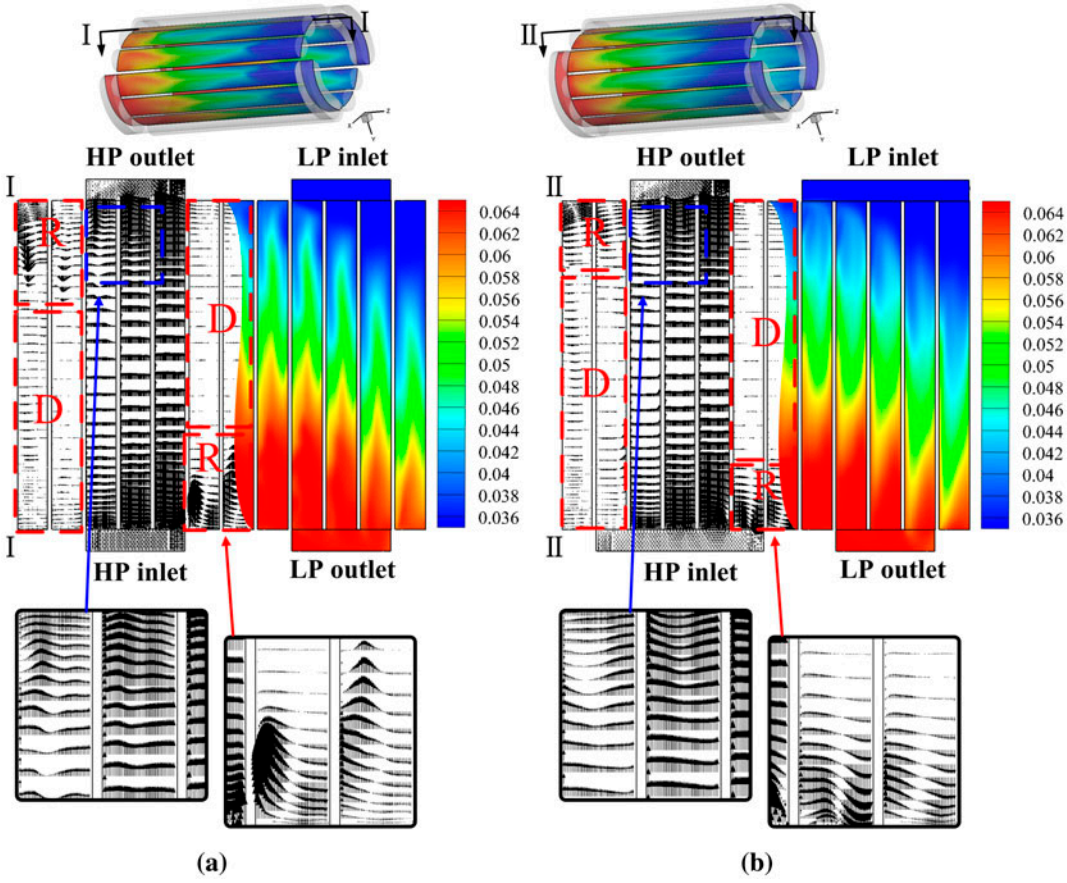

Fig. 10. Velocity vectors and concentration distribution with an extended angle of 0° (a) and ±30° (b).

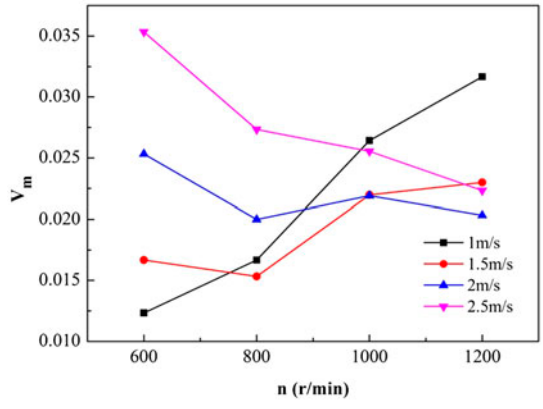

Fig. 11. Mixing rate in different operating conditions.

As shown in Fig. 11, an interesting trend reversal of mixing rate vs. rotary speed is observed when inflow velocity increases. At an inflow velocity of 1 m/s, the mixing rate increases with rotary speed, while decreases with rotary speed at a relative high inflow velocity of 2.5 m/s. Among them, the mixing rate fluctuates and no liner relationship is observed. This suggests that the mixing behavior is affected by a combination of the rotary speed and inflow speed, and an adjustable rotary speed can be used advantageously to control the mixing performance of RPE.

Fig. 12 presents the variation of mixing rate with oscillatory Reynolds number. The trend reversal phenomenon could be easily observed by extracting the two operating parameters. As shown in Fig. 12(a), with the decrease in rotary speed from 1,200 to 600 rpm, the slope of curve changes from negative to positive, and the mixing rate gradually shows a positive correlation with the increasing oscillatory Reynolds number. A similar trend is presented in Fig. 12(b), with the increase in inflow velocity, the correlation between oscillatory Reynolds number and mixing rate changes from negative to positive. It is indicated that there exits an optimal oscillatory Reynolds number to minimize the mixing rate. In this work, a minimum mixing rate is achieved at an oscillatory Reynolds number of about 178.

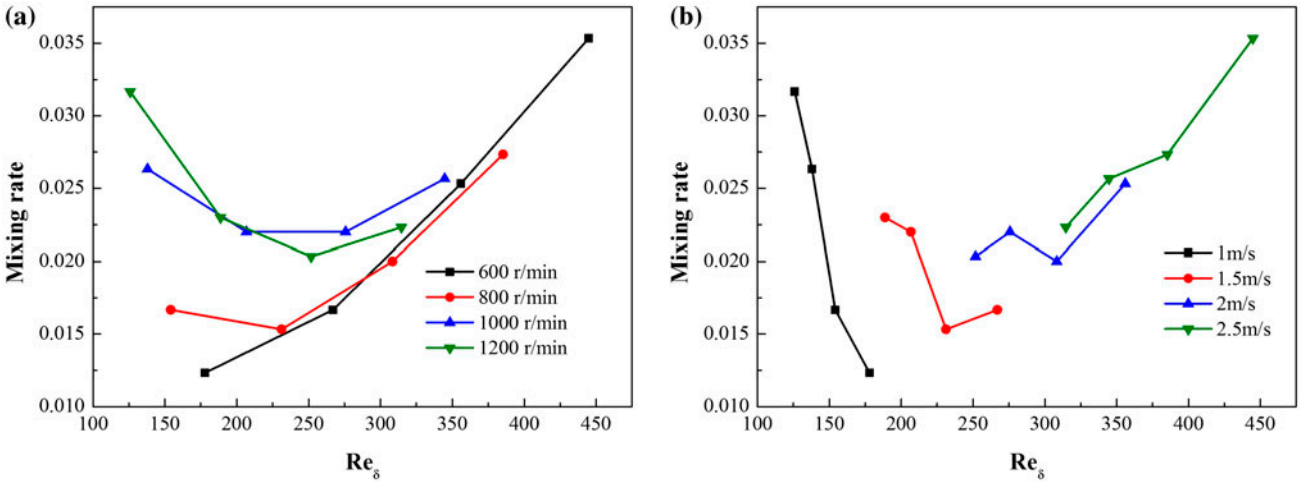

Fig. 12. The variation of mixing rate with oscillatory Reynolds number.

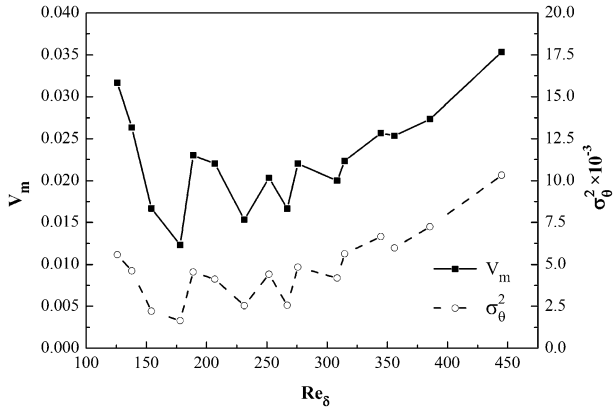

Fig. 13. Mixing performance and flow pattern in different operating conditions.

Based on the RTD analysis, the mixing rate and normalized RTD variance in different operating conditions are presented in Fig. 13. A good accordance between the two curves suggests that the RPE mixing performance has a close relationship with the flow pattern in various operating conditions. At an oscillatory Reynolds number of about 178, the normalized RTD variance is more close to 0, indicating the flow pattern is more close to the plug flow, which is believed to contribute to the minimum mixing rate of RPE.

6. Conclusions

In this study, an integration of CFD and RTD techniques was used to obtain the mixing performance and flow behavior of RPE devices. Based on a flow regime classification, the numerical simulation of unsteady flow in RPE was accomplished using laminar model. The effects of extended angle on the volumetric mixing rate and flow pattern were then investigated. In addition, the effect of various operating conditions was also discussed. And a close relationship of mixing performance with flow pattern in RPE was found using RTD analysis. The simulation result suggests that applying extended angle in RPE is beneficial to eliminate non-ideal flow structures caused by sudden opening and closing of ducts. The volumetric mixing rate for the extended angle of ±30° is the minimum compared with other RPE configurations in the present research. Besides, the mixing rate is minimized at an optimal oscillatory Reynolds number of about 178 in different operating conditions. A strong positive correlation was found between volumetric mixing rate and the RTD variance, which could be concluded that the smaller the variance, the more likely the flow pattern in RPE will tend to a plug flow, thus the lighter mixing could be achieved. The detailed information of the flow field in RPE was presented and was used to validate the flow pattern identification in RTD analysis. The combined of CFD and RTD technique applied in this work may be a viable method to study the mixing and flow behavior in RPE, and will provide preliminary insights for flow pattern optimization and mixing control.

Acknowledgment

This work was supported by the National Natural Science Foundation of China (Grant No. 21376187).

References

[1] R.F. Service, Desalination freshens up, Science 313 (2006) 1088–1090.

[2] K. Thu, K.C. Ng, B.B. Saha, A. Chakraborty, S. Koyama, Operational strategy of adsorption desalination systems, Int. J. Heat Mass Transfer 52(7–8) (2009) 1811–1816.

[3] M. Elimelech, W.A. Phillip, The future of seawater desalination: Energy, technology, and the environment, Science 333 (2011) 712–717.

[4] R.L. Stover, Seawater reverse osmosis with isobaric energy recovery devices, Desalination 203(1–3) (2007) 168–175.

[5] R.L. Stover, Retrofits to improve desalination plants, Desalin. Water Treat. 13(1–3) (2010) 33–41.

[6] E. Spiritos, C. Lipchin, in: N. Becker, Global Issues in Water Policy, vol. 4, in: Water Policy in Israel, Springer Science + Business Media, Dordrecht, 2013, pp. 101–123.

[7] L.F. Sotoft, K.V. Christensen, R. Andrésen, B. Norddahl, Full scale plant with membrane based concentration of blackcurrant juice on the basis of laboratory and pilot scale tests, Chem. Eng. Process. 54 (2012) 12–21.

[8] R.L. Stover, Development of a fourth generation energy recovery device. A 'CTO's notebook', Desalination 165 (2004) 313–321.

[9] Y. Zhou, X.-W. Ding, M. Ju, Y.-Q. Chang, Numerical simulation on a dynamic mixing process in ducts of a rotary pressure exchanger for SWRO, Desalin. Water Treat. 1 (2009) 107–113.

[10] Y. Liu, Y.-H. Zhou, M.-S. Bi, 3D numerical simulation on mixing process in ducts of rotary pressure exchanger, Desalin. Water Treat. 42(1–3) (2012) 269–273.

[11] E. Xu, Y. Wang, L. Wu, S.-C. Xu, Y.-X. Wang, S.-C. Wang, Computational fluid dynamics simulation of brine-seawater mixing in a rotary energy recovery device, Ind. Eng. Chem. Res. 53(47) (2014) 18304–18310.

[12] C.C. Mei, Y.-H. Liu, A.W-K. Law, Theory of isobaric pressure exchanger for desalination, Desalin. Water Treat. 39(1–3) (2012) 112–122.

[13] O.M. Al-Hawaj, The work exchanger for reverse osmosis plants, Desalination 157(1–3) (2003) 23–27.

[14] M. Hino, M. Sawamoto, S. Takasu, Experiments on transition to turbulence in an oscillatory pipe flow, J. Fluid Mech. 75(2) (1976) 193–207.

[15] D. Das, J.H. Arakeri, Transition of unsteady velocity profiles with reverse flow, J. Fluid Mech. 374 (1998) 251–283.

[16] R. Akhavan, R.D. Kamm, A.H. Shapiro, An investigation of transition to turbulence in bounded oscillatory Stokes flows Part 1. Experiments, J. Fluid Mech. 225 (1991) 395–422.

[17] C.V. Kerczek, On the Stability of Stokes Layers, Doctor Thesis, The Johns Hoplrins University, USA, 1973.

[18] V. Pikalov, S. Arrieta, A.T. Jones, J. Mamo, Demonstration of an energy recovery device well suited for modular community-based seawater desalination systems: Result of Danfoss iSAVE 21 testing, Desalin. Water Treat. 51(22–24) (2013) 4694–4698.

[19] ERI Energy Recovery Inc., Installation, Operation & Maintenance Manual 65-Series Pressure Exchanger Energy Recovery Devices ERI®Document Number 80019-01 Revision 8, San Leandro, 2008.

[20] S. Oh, S. Wang, M. Park, J. Kim, Topology optimization of spacers for maximizing permeate flux on membrane surface in reverse osmosis channel, Proceedings of the ASME 2011 International Design Engineering Technical Conferences & Computers and Information in Engineering Conference, Washington, DC, USA, 2011.

[21] P.V. Danckwerts, Continuous flow systems, Chem. Eng. Sci. 2(1) (1953) 1–13.